Tellus (1981), *33*, 552–563

Direct production of droplets from breaking wind-waves —its observation by a multi-colored overlapping exposure photographing technique

By MOMOKI KOGA, *Physical Oceanography Laboratory, Geophysical Institute, Tohoku University, Sendai 980, Japan*

(Manuscript received October 14, 1980; in final form March 6, 1981)

ABSTRACT

The micro-scale configurations of the surface of breaking wind-waves and their processes of change were investigated through wind-wave tank experiments, with use of a simple, new photographic technique of multi-colored overlapping exposures. The most conspicuous micro-scale phenomenon was the appearance of small projections, mainly on the crest of the wave and the succeeding stretching and breaking of these projections into small droplets. This sequence of events shows the process of the direct production of droplets by breaking waves. The movements of such directly produced droplets were also measured and their characteristics in relation to the phase of the wave are discussed.

1. Introduction

The microstructure of a breaking wind-wave's surface, including the whitecaps, has profound effect on the sea surface roughness, the exchange of heat and gases between the water and the air and on the microwave emissivity of the sea surface. There have been some wind-wave tank experiments with respect to the microstructure of nonbreaking wind-wave surfaces, such as distribution of surface slope, the number distribution of ripples along the phase of their carrier waves and the shapes of these ripples (e.g. Cox, 1958; Schooly, 1960; Keller and Wright, 1975; Lee, 1977; Wu, 1979). However, experiments regarding the microstructure of a breaking wind-wave surface are limited. Toba (1961) made a detailed photographic study and showed that the breaking wind-waves were profusely and widely covered with small-scale irregular rough areas. They were also covered with bubbles entrained from the trough area of Crapper-type small waves in the vicinity of the crest of their carrier wave.

The difference between sea surface states with and without whitecaps has often been discussed ever since Munk (1947). The microstructure of a wind-wave surface as well as the structure of the wind field near the wind-waves are much different in the two cases. These differences are reflected in the abrupt increase of the drag coefficient of the sea surface associated with the onset of whitecapping (e.g. Toba and Kunishi, 1970). The microstructure of a breaking wind-wave surface can thus not be understood as an extension of the nonbreaking case. Detailed measurements of the microstructure itself are indispensable for the exact understanding of the surface condition of breaking waves.

In this paper, a new, simple photographic technique of multi-colored overlapping exposure is devised and employed in photographing the micro-scale configurations of the surface of a breaking wind-wave during a strong wind. The sequence of events including the bubble formation and direct production of droplets is also investigated. Based on the analysis of photographs, the characteristic micro-scale phenomena along the breaking wind-wave surface are described in detail. Moreover, we intend to seek some answer to the confusing question "What constitutes a breaking wind-wave in the usual sense?", through the present experimental results related mainly to bubble entrainment and direct production of droplets.

2. Multi-colored overlapping exposure technique (MOET) and wind-wave tank experiment

Photographic methods are most suitable for the measurement of micro-scale shapes such as those over a wind-wave surface. If the micro-scale shapes are rapidly changing, high-speed motion cameras are usually used for the measurement of their prompt changes. A new photographic technique has been used, in which a still camera, or a cinecamera with standard speeds, can be successfully used to photograph the rapid changes. This photographic technique is an overlapping photographing technique which uses multiple strobes, flashing one after another at short intervals through optical filters of different colors. Using this technique, images of splashing droplets or of micro-scale configurations of wave surface at different instants are photographed in one picture, and the time sequences between the overlapping exposed images can easily be determined by their colors. Hereafter, this photographic technique is called "Multi-colored overlapping exposure technique (MOET)".

Color films usually have three color sensitivity layers, corresponding to the three primary colors, blue, yellow and red. For the correct discrimination of the time sequence of the overlapping images, two or three overlapping exposures may be appropriate. From the double overlapping exposure, velocity of the movement of the micro-scale shape can be measured. From the triple overlapping exposure, the acceleration can also be measured. This MOET can also be used for comparatively precise measurements of velocity vectors of fluid particles, including tracer particles in flow visualization studies.

In the present experiment, two color strobes, red and blue, were used for MOET. The "Shadowgraph photographic method" (Toba, 1961; Monahan, 1968; Koga and Toba, 1981) was also used at the same time to get distinct outlines of images near the breaking wind-wave surface, including small bubbles and droplets. A view of the photographic system from the top is shown in Fig. 1. In the

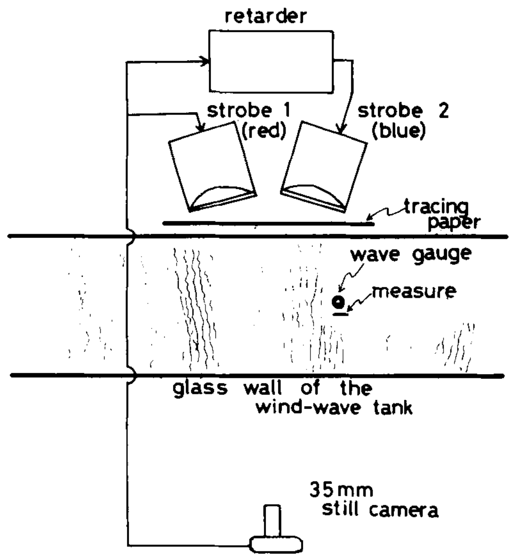

Fig. 1. Schematic representation of the photographic arrangements (top view) for the multi-colored overlapping exposure technique (MOET).

shadowgraph photographic system using the two-color overlapping exposure technique, each of the strobes directly flashes towards a 35-mm still camera through the measuring section of the tank, as shown in Fig. 1. A sheet of tracing paper is put on the glass wall of the tank on the side of the strobes for diffusing the light. The flashing time of the strobe (Sugawara Laboratories, Inc., Type PS-240) is about 27 μs. The time interval between the flashing of the two strobes was controlled by a signal retarder (Sugawara Laboratories, Inc., Type RE-130G). For measuring the movement of micro-scale configurations of a breaking wind-wave surface, entrained bubbles and splashing droplets, the flashing interval was fixed to the range of 2–8 ms; 5 ms was used most of the time.

The wind-wave tank used was 20 m long, 60 cm wide, 120 cm high with fresh water of 60 cm depth. A wave gauge and a measure were set up at the downwind end of the photographed area, as shown in Fig. 1, and the time marks of photographing were also recorded simultaneously with wave records.

Experimental conditions are shown in Table 1, together with the characteristic values of significant waves. A reference wind speed U_r was measured at the center of the upstream end section. The mean phase speed C of a wave was calculated from the

Table 1. *Experimental conditions at the time of direct production of droplets*

Reference wind speed U_r (m s^{-1})	Fetch F (m)	Friction velocity of air u_* (cm s^{-1})	Roughness length Z_0 (cm)	Significant wave Height $H_{1/3}$ (cm)	Significant wave Period $T_{1/3}$ (s)	Mean phase speed of wave c (cm s^{-1})
16.0	16	197	0.80	9.0	0.73	125
16.0	12	—	—	7.7	0.62	119
16.0	9	—	—	6.6	0.57	101
16.0	5	—	—	4.3	0.44	94
15.0	16	148	0.40	8.2	0.68	116
14.0	16	124	0.26	7.5	0.61	110

time lag of the wave records measured at two points separated by nearly a half wave length, though the local propagating speed of the wind wave surface was determined from the pictures of the MOET.

The general states of the air-water interface of the experiment are as follows. For the case of fixed wind $U_r = 16$ m s^{-1}, occurrence of wave breaking with bubble entrainment was seen rarely with a fetch of 5 m, but occurred frequently with a fetch of 16 m. On the other hand, for the cases of a fixed fetch of 16 m, the critical wind speed for the occurrence of wave breaking was $U_r = 12$ m s^{-1}. Wind conditions U_r during the photographing were 14, 15 and 16 m s^{-1}, which were larger than the above critical wind speed. These fairly strong winds were used to get occasional breaking of wind-waves in a region of short fetches. In such cases, the wave age C/U will be small and the effects on the surface drift current will be large, compared to the case of ocean waves. However, the micro-scale phenomena of the breaking wind-wave surface which have been revealed in the present experiment, such as the direct production of droplets, should be equally important, especially for the higher frequency part of ocean wind waves.

The photographs were analyzed in the following way. Each of 35-mm negatives was projected onto a large sheet of paper, and the outlines of micro-scale configurations of the wave surface and images of the droplets and bubbles in focus were traced on the paper. The minimum size of the droplets and bubbles which can be precisely judged on the photographs of 35 cm × 52 cm was about 0.8 mm in diameter. This lower limit was decided mainly by the focal depth of field. As the pictures were taken with a telephoto objective lens with close-up rings, the size error arising from the field angle of the lens can be regarded as small. This size error was at most 13 % in this study.

3. Some representative phenomena on and near the surface of breaking wind-waves

The photographs taken by MOET (Figs. 2a and b) show the breaking of wind-waves accompanied by bubble entrainment and direct production of droplets. The flashing interval t of the two lights is 5 ms, and the wind direction is from left to the right. The pictures show the shadow image. The successive two images are seen by blue and red colors, in the opposite order to the flashing order of red and blue lights, since shadow images are colored by the light when there is no obstacle. The images of bubbles, droplets and of wave surface are transparent to a certain degree, as they are of transparent matter and only their marginal region makes an impact on the photographing film due to reflection and refraction of light.

With the aid of these photographs, the following items can be investigated in detail: (1) appearance and development of micro-scale irregular shapes on the breaking wave surface, (2) direct production of the droplets by breakup of these irregular shapes, and (3) their diffusion processes.

In this paper, the above series of phenomena are examined. Although the entrained bubbles are also seen in these photographs, the process of bubble entrainment and their diffusion in water will be described elsewhere.

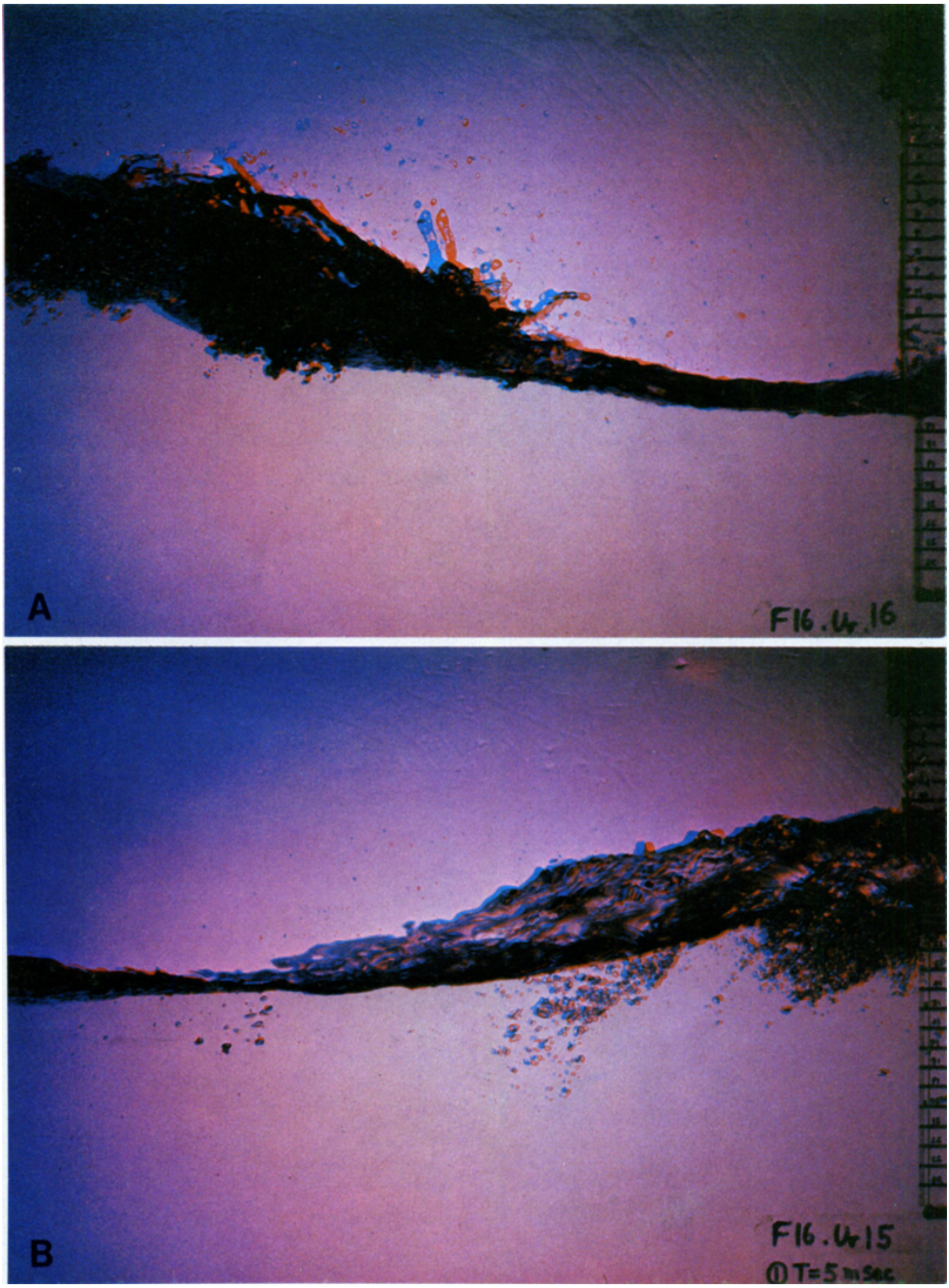

Fig. 2. Photographs by MOET (two-colour). Wind direction is from left to right. Successive two images are shown by blue and red colors. One division of the photographed measure (right end) is 1 cm. (a) Fetch $F = 16$ m, representative wind velocity $U_r = 16$ m s^{-1}, flushing interval $t = 5$ ms. (b) $F = 16$ m, $U_r = 15$ m s^{-1}, $t = 5$ ms.

3.1. *The appearance of small projection on wave surface*

The wind-wave surface during light winds is generally smooth, especially on its windward side, though small ripples are trapped on the downwind surface close to the crest (e.g. Cox, 1958; Wu, 1979). On the other hand, during the strong wind conditions encountered in the present experiment, there is the occasional appearance of whitecaps, and the wind-wave surface is completely covered with irregular small rough areas (e.g. Toba, 1961). The most characteristic phenomenon related to the microstructure of the wind-wave surface under these strong wind conditions is the appearance of small projections. These projections are isolated and three-dimensional with shapes like a hanging bell, with occasional stretching of the "bell" form.

In Fig. 2a fully stretched projections are seen on the downwind slope of the wind-wave. Although these projections are concentrated mainly on the downwind slope and the crest, they may sometimes appear on the upwind slope. In Fig. 2b some distinct projections are visible on the upwind slope of the wave. Careful inspection of the photographs reveals that the appearance of projections does not necessarily require the occurrence of breaking accompanied by bubble entrainment, or splashing at the very crest.

Hereafter, a quantitative description of the shape of projection in terms of its size λ and the steepness δ will be discussed in detail. The size λ is defined as the distance across the base of the projection and the steepness δ is defined as the ratio of the height h to the size λ. In the course of the analysis of photographs, a small irregular shape on the wave surface is identified as a projection if it is isolated and if δ is larger than about 0.2. Fifty photographs were analyzed for the case $U_r = 16$ m s^{-1}, $F = 5$ m and 36 photographs for the remaining cases.

The distribution of the size of the projection λ measured from the photographs is shown in Fig. 3a for the case $U_r = 16$ m s^{-1}. The range of λ is from 0.5 cm to 2.5 cm, with most values around 1.0 cm. As far as the present experimental data are concerned, no systematic differences in the range and characteristics of the distribution are found with varying wind speed and fetch. Fig. 3b shows the relation in summarized form between the size λ and the steepness δ of the projection for all experimental conditions, excluding the extremely stretched projections which seem to be about to break up. For the representative value of λ, say 1.0 cm, δ ranges mostly from 0.4 to 0.6. For smaller λ than the representative value, δ ranges to about 2.0. It is seen from Fig. 3b that δ shows an inverse

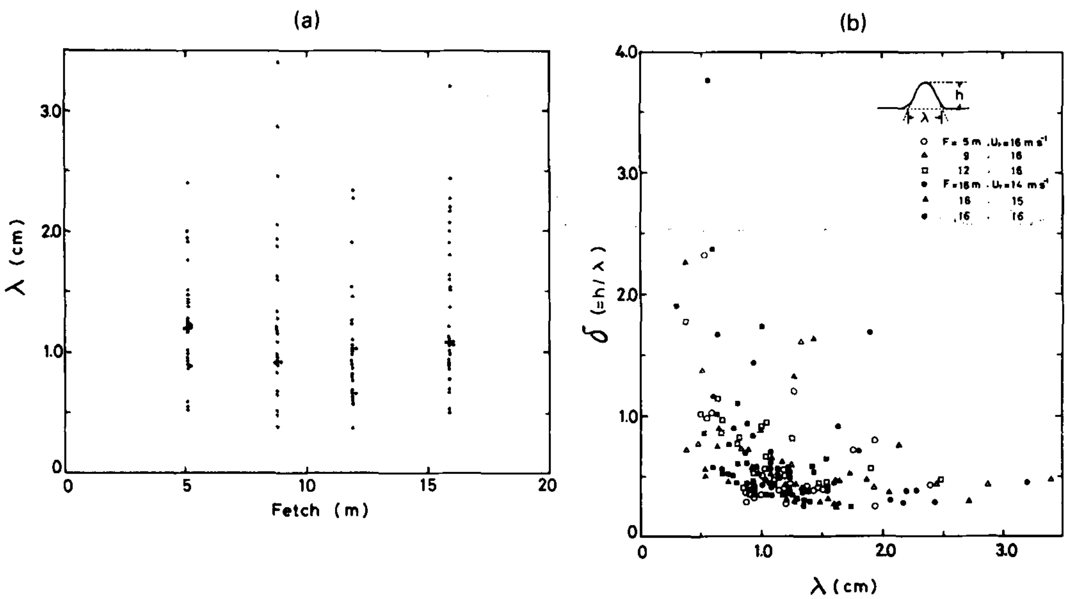

Fig. 3. Size distribution of projections. (a) Size of projection λ plotted against fetch for $U_r = 16$ m s^{-1}. (b) Relation between size λ and steepness of projection δ.

relation to λ and this suggests that the projections grow more slender as they stretch upward.

In the present photographic technique, changing processes and speed of projections can also be measured together with their static shapes. In Fig. 4a, the distribution of horizontal moving speed U_p of the projection at each fetch is represented for the case $U_r = 16$ m s^{-1}. It should be mentioned here that the phase speed of the individual wind waves corresponding to each of the pictures was not measured at the same time. However, supplementary measurements of the phase speed of the waves show that the standard deviation of the phase speed distribution of individual wind-waves is about 10%. Therefore, the mean phase speed C can be used in the following discussions, and the value is entered in Fig. 4a by horizontal bars. U_p is generally larger than C, and the variation of U_p with the fetch has a similar trend to that of C. The probability distribution of normalized moving speed U_p/C is shown in Fig. 4b. The U_p/C ranges from 0.5 to 2.5, with the maximum probability at about 1.2. Therefore, it can be said that most of these projections are standing or moving forward, relative to their carrier waves. Considering the fact that most stretched projections are seen at the leading slope of wave near to the crest, the following process is expected. Some of these projections also grow up in the manner of stretched millet jelly, as they are proceeding forward relative to their carrier waves. Such a change in the form of the projection leads to the process of direct production of droplets, which will be discussed in the following section.

3.2. *Direct production of droplets*

The photographs show that droplets are directly produced by the breakdown of fully stretched small projections. Fig. 5 exhibits the process. The thick solid line indicates the outline of the first images and the dotted line or the thin solid line the second images. The formation of a slightly curved array of droplets in Fig. 5 (especially 5b), indicates that these droplets are produced by the breakdown of the above-mentioned fully stretched small projections. The maximum size of the directly produced droplets was about 3.0 mm in diameter in the present case. This sequence of events, i.e. the appearance of a projection, its stretching and breaking to small droplets, is very similar to the splashing phenomena on the surface of a water jet ejected through a nozzle at high speed, which was investigated by Hoyt *et al.*, 1974, and Hoyt and Taylor, 1977.

In the present study, the direct production of droplets was seen mostly near the crest on the leading slope of the carrier wave, with an occasional appearance of it on the windward slope near the crest, as shown in Figs. 5a and 5b. In the latter case, it was seen that droplets were produced in a shorter time than in the former.

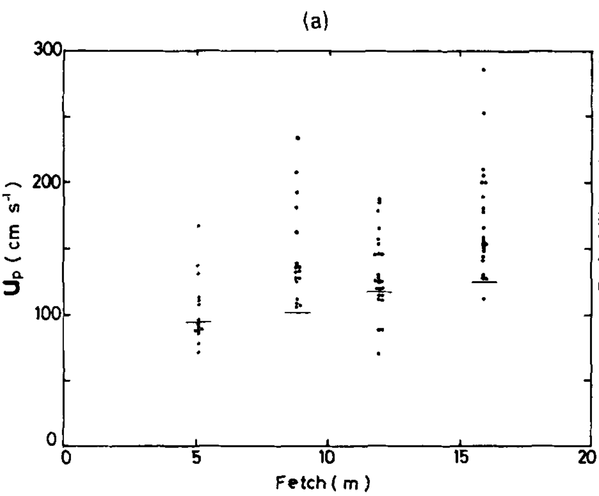

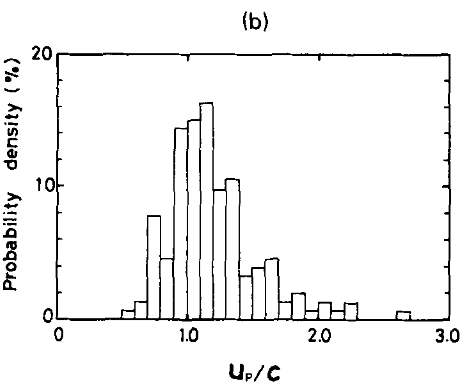

Fig. 4. Distribution of horizontal speed of projections. (a) Horizontal speed of projection U_p plotted against fetch for $U_r = 16$ m s^{-1}. Horizontal short lines indicate the representative phase speed of waves C at respective fetches. (b) Probability distribution of U_p/C.

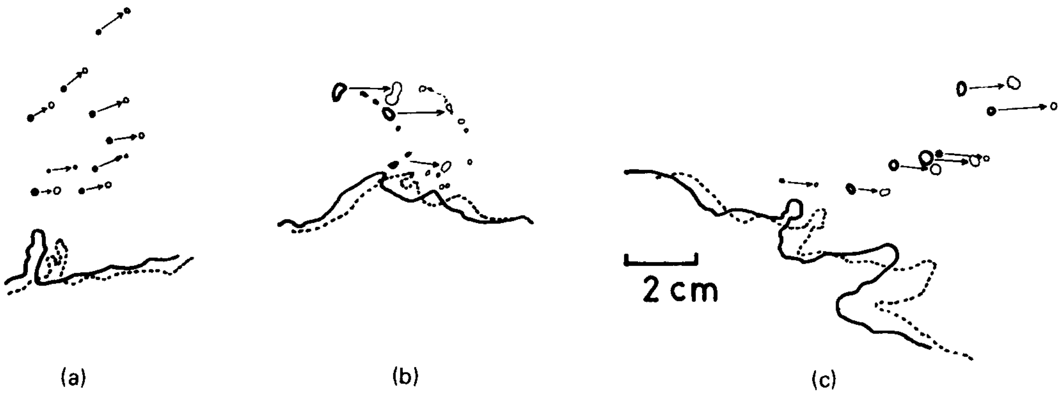

Fig. 5. Pictures of direct production of droplets traced from photographs of MOET (two-color). Thick solid line indicates first time images and dotted line or thin solid line indicate second time images. (a) Windward slope near the crest $F = 5$ m, $U_r = 16$ m s^{-1}, $t = 6$ ms. (b) At the crest $F = 16$ m, $U_r = 16$ m s^{-1}, $t = 5$ ms. (c) Leading slope near the crest $F = 9$ m, $U_r = 16$ m s^{-1}, $t = 5$ ms.

As to mechanisms of droplet production, it has been pointed out (Blanchard and Woodcock, 1957; Toba, 1961) that droplets are produced by two mechanisms, first by the bursting of entrained bubbles at the wave surface (mainly for smaller droplets) and second by splashing (mainly for larger droplets). The breaking down process of projection discussed here may give a clearer image of the direct production of droplets by the splashing mechanism.

In the following paragraphs, the relationship between the size ranges of droplets produced by these two mechanisms is examined. It has been pointed out that the largest size of a droplet produced by the bursting of bubbles would be at most about 0.5 mm in diameter (Blanchard and Woodcock, 1957; Hayami and Toba, 1958; Toba, 1959). Therefore, most of the droplets larger than 0.5 mm in diameter, measured near the wave surface, are produced by the mechanism of direct splashing in the manner that has been described above. Koga and Toba (1981) measured droplet distribution near the wind-wave surface by using a wind-wave tank, and showed that droplets of all sizes in the range of 30 μm to 2 mm in diameter were produced, though their number density decreased with an increase of their size by a power law relation. From these observations, it can be expected that the size ranges of droplets produced by the two mechanisms, i.e. bursting of bubbles and direct splashing, will fully overlap each other. This is well supported by the present experiments, by the presence of many out of focus droplets near breaking projections. The size of

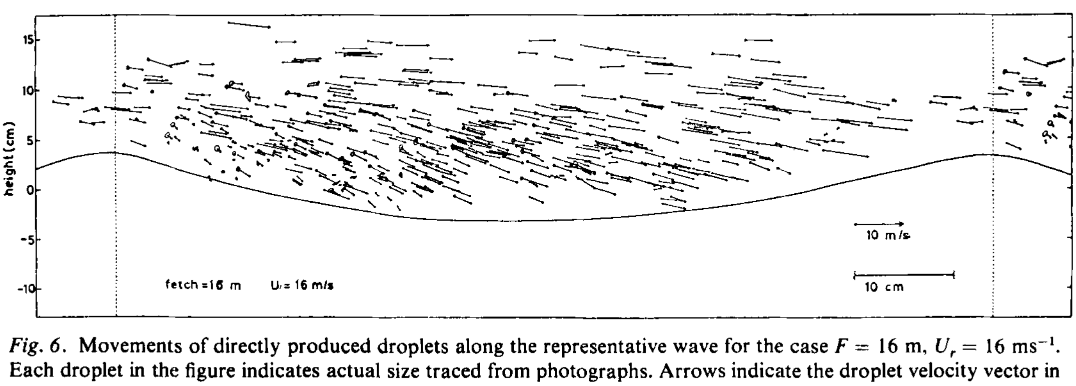

Fig. 6. Movements of directly produced droplets along the representative wave for the case $F = 16$ m, $U_r = 16$ ms^{-1}. Each droplet in the figure indicates actual size traced from photographs. Arrows indicate the droplet velocity vector in a coordinate moving with the phase speed of the wave.

these droplets seemed to be much smaller than 0.8 mm in diameter, the present lower limit of analysis.

3.3. *Movement of droplets*

Droplets produced by the process described above spread upward partly by air turbulence and partly by forward acceleration due to mean wind which increases with height. The spreading mechanism of the droplets varies according to the size of the droplets, as discussed by Koga and Toba (1981). For droplets with a diameter of 150 μm or more, the diffusion by air turbulence is not of great importance, but their initial speed at the instant of their production and the acceleration by wind are important.

We now concentrate on the movement of droplets with a diameter larger than 0.8 mm (lower size limit of the present analysis). The distribution of the velocity vector of the splashing droplets relative to the wave profile was prepared by overlapping photographs. The result is shown in Fig. 6 for the case of $U_r = 16$ m s^{-1}, $F = 16$ m. Based on Fig. 6 and on the previous results regarding the direct production of droplets, the mean features of the movement of the splashing droplets can be outlined. Most of the droplets (>0.8 mm in diameter) are produced on the leading slope near the crest of wave, with initial speeds of the same order of, or somewhat larger than, the speed of the projection. They spread upward and forward by the acceleration due to the drag by the mean wind. Due to gravity most of them return to the water surface on the windward slope near the crest of the next wave, their trajectories through the air making an angle of nearly 15 degrees with the horizontal. Their short life span may be due mainly to an insufficient acceleration by the mean wind.

The above fact may be made more clear by a comparison of the droplet velocity and the local wind speed. The mean horizontal wind speeds at 11 and 15 cm height above the still water surface were 13.3 and 14.4 m s^{-1}, respectively. At heights lower than 10 cm, the mean wind speed could not be measured due to clogging of the Pitot-static tube head with droplets. However, in this region, where most of the splashing droplets are distributed, the wind speed is expected to be around 12.0 m s^{-1} assuming a logarithmic wind profile down to the wave surface. From the figure it is seen that most of the droplets collide with the wave surface when they are accelerated to about half of the local wind speed.

In some cases, the photographs show the jumping of small droplets over the next crest, though this phenomenon is not clearly seen in Fig. 6. This is especially evident in the case when the steepness of the next crest is large; even large droplets sometimes jumped upward with some inclination over the next crest. This observation implies the existence of a strong jet flow near the crest, as pointed out by Chang *et al.* (1971). On the other hand, on the leading slope of the wave near the crest, the droplet velocity is generally small. This is the case even for small droplets. This may be accompanied by air flow separation the occurrence of which is to be expected above the leading slope of the wave.

Few measurements of droplet velocity distributions have been done. Wu (1973) and Macha (1979) made some, although they concentrated their measurements on the number and size distributions of droplets. Wu (1973) measured the velocity of a droplet of about 200 μm with a laser and phototransister unit. Macha (1979) measured the total number of fluxes of large droplets, as well as their mass and momentum fluxes, and estimated the representative velocity of the droplets. The velocity distribution and the outlines of splashing trajectories of droplets larger than 0.8 mm in diameter have been measured in the present work for the first time, along the wave profile including the trough area. The movement of splashing droplets is strongly influenced by the acceleration by the mean wind and by gravity. In order to get a clear understanding of the movement of splashing droplets, it is therefore essential to know the local wind distribution close to the breaking wind-waves which are accompanied by the direct production of droplets. This will be treated in a succeeding paper.

4. Creation mechanism of projections and the condition of wave breaking

Small projections on the surface of a wind-wave during strong winds, such as the ones shown in Fig. 2, are clearly different from the ripple waves. These projections have distinctive shapes and exist in isolation from each other in most cases. These projections move with a speed close to the phase speed of the carrier wave, and conserve their characteristic shapes. In this case, the substantial fluid elements constituting these projections seem to move with the same speed as the projections.

Kelvin-Helmholtz instability, in which instability of small disturbances occurs by the excess of air suction which overtakes the restoring force of wave motion, may be considered as a suitable model for the creation mechanism of these projections. With this mechanism, the destabilization of small disturbances is inevitably accompanied by the disappearance of their propagative nature as waves. However, in the present experiment, projections move with a speed similar to the phase speed of the wave, as shown in Figs. 4a and b. During this situation, the moving speed of projection can be interpreted as a reflection of the local wind drift along the wave surface.

Hereafter, the ability to create projections is examined by the use of the Kelvin–Helmholtz type instability model, including the shear effect of the wind profile, that was proposed by Miles (1959). In Miles' model, the critical condition for Kelvin–Helmholtz instability is given as,

$$C_0^2 = sU_1^2[\tfrac{1}{4}\pi^2 + \ln^2(2\gamma kZ_0)] \quad (1)$$

where,

$$C_0^2 = \frac{(\rho_+ - \rho_-)g + Tk^2}{(\rho_+ + \rho_-)k}$$

$$s = \rho_+/\rho_-$$

$$U_1 = U_*/K.$$

The symbol k represents the wave number of the disturbance, g is the acceleration of gravity, T is the surface tension, ρ_- and ρ_+ are the density of the fluid of the lower and the upper layer respectively, K is von Kármán's constant, γ is the universal constant of 1.78 ($\ln \gamma$ denotes Euler's constant), and Z_0 is the roughness length. The physical meaning of eq. (1) is easily understood when both sides of it are multiplied by ρ_-. Then, the right-hand side of eq. (1) represents the aerodynamic suction $-P_a$ and the left-hand side ($\rho_- C_0^2$) represents the restoring force both by the acceleration of gravity and by the surface tension. Instability occurs when the aerodynamic suction is larger than the restoring force.

With eq. (1), we can examine the stability of small disturbances of various wave numbers under given wind condition, U_* and Z_0. These values of U_* and Z_0 are calculated by the wind profile for each wind condition. In Fig. 7, the right-hand side of eq. (1), $-P_a/\rho_-$, is compared with that of C_0^2, for various wind conditions. For the present case, the critical condition occurs when U_r is larger than about 14 m s^{-1} and the wave number is also of the same order as that of the projections, as shown in Fig. 7.

Miles' model has been modified by including the effect of a surface drift current in the place of the zero assumption in the model. Though the real surface drift has a shear structure, it is considered as being uniform as a first approximation in the estimation of the effect of drift on the creation of projections. The effect of a simple uniform drift current is easily estimated on the bases of Miles'

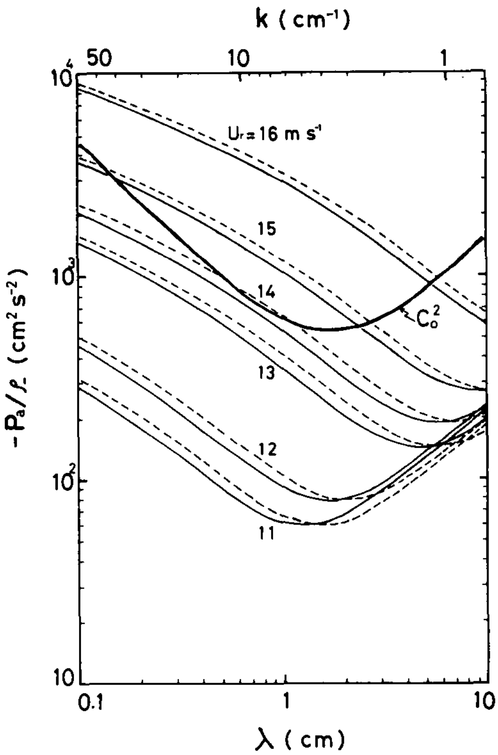

Fig. 7. Comparison between $-P_{as}/\rho_-$ and C_0^2 for various λ or k. The distribution of $-P_a/\rho_-$ estimated by Miles' (1959) model for various wind speeds U_r is shown by a thin solid line and the distribution of C_0^2 by a thick solid line. The modified estimation of $-P_a/\rho_-$, using the right-hand side of eq. (2), is also shown by a thin dashed line for the case $q = 0.5\ U_*$.

(1959) model. In this case, Miles' condition for occurrence of instability is modified as

$$C_0^2 = sU_1^2[\tfrac{1}{6}\pi^2 + \ln^2(2\gamma kZ_0)] + 2sqU_1 \cdot \ln(2\gamma kZ_0) + sq^2 \quad (2)$$

where q is a uniform drift current. Experimental data (Wu, 1975; Okuda, 1980) suggest that the surface drift current could be represented by $0.5\ U_*$.

Fig. 7 shows that destabilization of the disturbance is prompted to some extent by the presence of a surface drift current. However, the critical wind speed is not very different from that estimated by the original Miles' model. According to the present Kelvin-Helmholtz instability model, it is expected that the critical condition is satisfied when U_r is larger than 14 m s^{-1}.

In reality, however, direct splashing of droplets and bubble entrainment occurred at wind speeds greater than about 12 m s^{-1} along with the appearance of projections. This difference indicates that the instability occurs locally near the wave crest at lower values of U_r than those predicted by eqs. (1) and (2). This is as a result of the presence of localized high wind shear at the upwind slope near the crest as pointed by Chang *et al.* (1971). The presence of local high wind shear can also be supported by the manner of splashing of the droplets, as mentioned in the previous section. This evidence may be consistent with the fact that projections cannot be seen at the wave surface in the trough region, even at $U_r = 16$ m s^{-1}.

Moreover, a wind-induced high shear flow structure of the surface drift current whose effect is not included in the present model, may influence both the critical wind condition for instability and the scale of the disturbances. Although there remain some problems such as the above, it seems to be appropriate to consider that the main mechanism for the creation of projections is the Kelvin-Helmholtz instability.

Let us now look at the relation between the condition for splashing by the above-stated mechanism and the generally accepted condition for spilling breakers (the surface current U_s exceeds the phase speed of wave C). The previous discussion regarding the mechanism for the creation of projections clearly indicates that the surface drift current under a projection also has the same velocity as the projection itself. Therefore, it can be easily expected that the surface drift current exceeds the phase speed of the wave widely around the crest, since some projections around the crest exceed the phase speed in many cases. The condition $U_s \geq C$ is essential for the growth of a projection, because this condition enables the projection to stay near the crest where the energy of the wind is most effectively transferred to the projection. This is consistent with the fact that most projections are seen near the crest. From this point of view the condition that $U_s \geq C$ is recognized as a necessary one for the effective growth of projections. However, careful inspection of the present photographs shows that the presence of projections with greater speed than the phase speed is not always accompanied by a simultaneous direct production of droplets. This observation shows that the presence of surface drift current exceeding the phase speed of the wave, $U_s \geq C$, does not necessarily mean the occurrence of wave breaking accompanied by direct production of droplets.

The above discussion with respect to the condition for wave breaking may be concluded as follows: the occurrence of such a wave breaking, overtaking the restoring force by the acceleration of gravity and surface tension (i.e. the development of Kelvin-Helmholtz instability) is another step after the appearance of the stagnation point on a wave surface (condition $U_s \geq C$). This would not contradict the suggestion of Banner and Phillips (1974), that the occurrence of breaking itself seems to be far more widespread than the occurrence of whitecaps. Banner and Phillips defined wave breaking by the presence of a stagnation point, that is the condition $U_s \geq C$, on the surface of a steady wave train.

5. Concluding remarks

The mechanism of the direct production of droplets that has been described in the present paper, i.e. the stretching and breaking of projections, gives a concrete image and amends the previous vague image that water spills off from the wave crest when the surface wind drift exceeds the phase speed of the carrier wave.

The movement of directly produced droplets was also measured and their characteristics along the wave were discussed. Most of the droplets larger than 0.8 mm in diameter that are produced near the crest fall back to the windward side of the next crest because of the insufficient acceleration by mean wind.

The presence of the projections discussed above is one of the most distinct phenomena in a fully roughened surface of a wind-wave during strong winds. The fully roughened surface which is characterized by the presence of the projections is expected to affect the following process; the abrupt increase of drag coefficient with wave breaking, changes in heat and gas exchange at the air-water interface, and the microwave emissivity of the sea surface.

6. Acknowledgments

The author wishes to express his sincere thanks to Professor Y. Toba of Tohoku University for introducing him to this field of work and for constant valuable advice and encouragement. Thanks are also due to Dr S. Kawai and Dr K. Okuda of Tohoku University for their valuable suggestions and encouragement, and to Mr P. S. Joseph for his kind correction of the English.

REFERENCES

Banner, M. L. and Phillips, O. M. 1974. On the incipient breaking of small scale waves. *J. Fluid Mech. 65*, 647–656.

Blanchard, D. C. and Woodcock, A. H. 1957. Bubble formation and modification in the sea and its meteorological significance. *Tellus 9*, 145–158.

Chang, P. C., Plate, E. J. and Hidy, G. M. 1971. Turbulent air flow over the dominant component of wind-generated water waves. *J. Fluid Mech. 47*, 183–208.

Cox, C. S. 1958. Measurements of slopes of high-frequency wind waves. *J. Marine Res. 16*, 199–225.

Hayami, S. and Toba, Y. 1958. Drop production by bursting of air bubbles on the sea surface (I). Experiment at still sea water surface. *J. Oceanogr. Soc. Japan 14*, 145–150.

Hoyt, J. W., Taylor, J. J. and Runge, C. D. 1974. The structure of jets of water and polymer solution in air. *J. Fluid Mech. 63*, 635–640.

Hoyt, J. W. and Taylor, J. J. 1977. Waves on water jets. *J. Fluid Mech. 83*, 119–127.

Keller, W. C. and Wright, J. W. 1975. Microwave scattering and straining of wind-generated waves. *Radio Sci. 10*, 139–147.

Koga, M. and Toba, Y. 1981. Droplet distribution and dispersion process on breaking wind waves. *Sci. Rep. Tôhoku Univ., Ser. 5* (Tôhoku Geophys. Journ.) *28*, 1–25.

Lee, P. H. Y. 1977. Doppler measurements of the effects of gravity waves on wind-generated ripples. *J. Fluid Mech. 81*, 225–240.

Macha, J. M. 1979. The effects of spray entrainment on the mean wind profile and the overall load on marine structures. Aerospace Engineering Department, Texas A & M University, 88 pp.

Miles, J. W. 1959. On the generation of surface waves by shear flows. Part 3. *J. Fluid Mech. 6*, 583–598.

Monahan, E. C. 1968. Sea spray as a function of low elevation wind speed. *J. Geophys. Res. 73*, 1127–1137.

Munk, W. H. 1947. A critical wind speed for air-sea boundary processes. *J. Marine Res. 6*, 203–218.

Okuda, K. 1980. Study on the internal structure of wind waves. Ph.D. Thesis, Tohoku University.

Schooley, A. H. 1960. Double, triple and higher-order dimples in the profiles of wind-generated water waves in the capillary-gravity transition region. *J. Geophys. Res. 65*, 4075–4079.

Toba, Y. 1959. Drop production by bursting of air bubbles on the sea surface (II). Theoretical study on the shape of floating bubbles. *J. Oceanogr. Soc. Japan 15*, 121–130.

Toba, Y. 1961. Drop production by bursting of air bubbles on the sea surface (III). Study by use of a wind flume. *Memoirs Coll. Sci. Univ. Kyoto, Ser. A, 29*, 313–344.

Toba, Y. and Kunishi, H. 1970. Breaking of wind waves and the sea surface wind stress. *J. Oceanogr. Soc. Japan 26*, 71–80.

Wu, J. 1973. Spray in the atmosphere surface layer: Laboratory study. *J. Geophys. Res. 78*, 511–519.

Wu, J. 1975. Wind-induced drift currents. *J. Fluid Mech. 68*, 49–70.

Wu, J. 1979. Distribution and steepness of ripples on carrier waves. *J. Phys. Oceanogr. 9*, 1014–1021.

ПРЯМОЕ ОБРАЗОВАНИЕ КАПЕЛЬ ПРИ ОБРУШЕНИИ ВЕТРОВЫХ ВОЛНЕГО НАБЛЮДЕНИЕ С ПОМОЩЬЮ ФОТОГРАФИЧЕСКОЙ ТЕХНИКИ МНОГОЦВЕТНЫХ ПЕРЕКРЫВАЮЩИХСЯ ЭКСПОЗИЦИЙ

С помощью новой простой фотографической техники многоцветных перекрывающихся экспозиций в эксперименте в бассейне с ветровыми волнами исследовались микромасштабные конфигурации поверхности обрушивающихся волн. Наиболее примечательным эффектом, относящимся к микромасштабным конфигурациям, было появление небольших струй, в основном, с гребня волны и последующий процесс их растяжения и дробления в мелкие капли. Этот процесс, начиная с образования струи, видимый в данном эксперименте, представляет собой картину прямого образования капель при обрушении волн. Движения этих непосредственно образующихся капель были также измерены и обсуждены их характеристики в связи с фазой волны.